

Unveiling UV/IR Mixing via Symmetry Defects: A View from Topological Entanglement Entropy

Jintae Kim,^{1,*} Yun-Tak Oh,² Daniel Bulmash,^{3,4} and Jung Hoon Han^{1,†}

¹*Department of Physics, Sungkyunkwan University, Suwon 16419, Korea*

²*Division of Display and Semiconductor Physics, Korea University, Sejong 30019, Korea*

³*Department of Physics, United States Naval Academy, Annapolis, MD 21402, USA*

⁴*Department of Physics and Center for Theory of Quantum Matter,
University of Colorado Boulder, Boulder, Colorado 80309, USA*

(Dated: October 17, 2023)

Some topological lattice models in two spatial dimensions have been found to exhibit intricate system size dependence in their ground state degeneracy (GSD), often known as UV/IR mixing. We distinguish between two explanations for this phenomenon by explicitly calculating the topological entanglement entropy (TEE) of a model system, the rank-2 toric code, for a bi-partition of the torus into two cylinders. Focusing on the fact that the rank-2 toric code is a translation symmetry-enriched topological phase, we show that viewing distinct system sizes as different translation symmetry defects can explain both our TEE results and the GSD of the rank-2 toric code. Our work establishes the symmetry defect framework as the most complete description of this system size dependence.

In the realm of topological order in two dimensions, one may observe the emergence of anyonic excitations characterized by their anyonic braiding statistics and the topology-dependent ground state degeneracy (GSD) [1, 2]. In the presence of symmetry, the structure of topological order becomes even richer as there can be multiple distinct “symmetry-enriched topological phases” (SETs) with the same anyons and statistics [3–8]. SETs exhibit symmetry fractionalization [3, 9], wherein the emergent quasiparticles transform projectively under the symmetry operations. Furthermore, the symmetry may non-trivially permute the topological superselection sectors, which is denoted as anyonic symmetry [8, 10, 11].

Normally, the GSD of a topologically ordered system on a torus depends only on the number of distinct anyon types, which is independent of the system size. However, several models in which the GSD depends sensitively on the size of the torus have been discussed recently [12–25]. For example, the \mathbb{Z}_N plaquette model [12, 13] has a GSD which depends on whether the linear dimension is even or odd, while other \mathbb{Z}_N models have GSDs that depend on the linear dimension modulo N . This system size dependence has sometimes been viewed as a signature of so-called UV/IR mixing, in the sense that microscopic information (namely the lattice constant) affects the low-energy properties of the model.

There have been two primary explanations for the mechanism by which the system size affects the low-energy properties of topologically ordered systems. One [15, 20] is to view certain locally inequivalent configurations of excitations as globally equivalent thanks to processes that take place over the entire linear size of the system. Another [25] emphasizes the fact that these systems are translation SETs and views the system size

dependence as arising from translation symmetry defects threaded through non-contractible spatial cycles. Both of these explanations have been used to quantitatively explain the topological GSD of lattice anyon models.

In this work, we show that for one such model, the symmetry defect approach can explain not only the GSD but also the topological entanglement entropy (TEE) for the bi-partition of the torus into two cylinders [26–29]. This is strong evidence for the usefulness of the defect approach because if the entanglement cut has non-contractible loops, then the TEE allows us to directly extract the quantum dimension of symmetry defects. In contrast, because this TEE explicitly incorporates one periodic boundary condition but not the other, it is much less natural to justify the torus TEE via some global relation between superselection sectors. The model we choose is the \mathbb{Z}_N rank-2 toric code (R2TC) [17–20, 30]. We match our explicit calculation of the TEE and known results about the GSD to quantitative predictions from the theory of symmetry defects in SETs [10, 11, 31, 32]. From this perspective, different linear system sizes modulo N are viewed as having different symmetry defects threaded through a handle of the torus.

The R2TC is a generalization of the Kitaev toric code consisting of three types of stabilizers called a_i , b_i^x , and b_i^y , defined respectively around the site i and the two links $(i, i + \hat{x})$, and $(i, i + \hat{y})$ on a square lattice as shown in Fig. 1. At each site we have two \mathbb{Z}_N degrees of freedom, denoted by subscripts 1 and 2, with an additional \mathbb{Z}_N degree of freedom at the center of each plaquette denoted by the subscript 0. Using these \mathbb{Z}_N spins we can construct the three stabilizers as depicted in Fig. 1. The stabilizer a_i is a product of \mathbb{Z}_N Pauli-Z operators, while b_i^x and b_i^y are products of \mathbb{Z}_N Pauli-X operators, which form the algebra $Z_{i,a}X_{j,b} = \omega\delta_{ij}\delta_{ab}X_{j,b}Z_{i,a}$, where $a, b = 0, 1, 2$ and $\omega = e^{2\pi i/N}$. The ground state(s) is an eigenstate of all the stabilizers with the eigenvalue +1. Excitations of this model are anyons carrying *position-dependent* labels;

* Electronic address: jint1054@gmail.com

† Electronic address: hanjemme@gmail.com

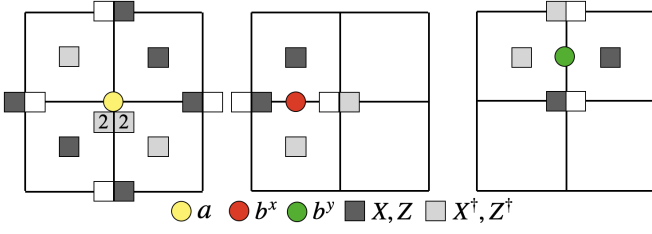


FIG. 1: Three stabilizers a_i , b_i^x , and b_i^y of R2TC are depicted as yellow, red, and green symbols, respectively. The a_i stabilizer is a product of \mathbb{Z}_N Pauli-Z operators, while b_i^x and b_i^y consist of \mathbb{Z}_N Pauli-X operators. There are two \mathbb{Z}_N spins defined at the vertices (represented by two adjacent squares) and one \mathbb{Z}_N spin (represented by a single square) at the plaquette centers of the square lattice. The ‘2’ inside the squares on the far left figure implies the action by $(Z^\dagger)^2$ for both spins. The empty square means there is no action by Pauli operators on that spin.

following [20], one can label the distinct anyon types at the site (i_x, i_y) using the formula

$$\begin{aligned} l_{i_x, i_y} = & l_1 \mathbf{e} + (l_1 i_x + l_2 \bmod N) \mathbf{p}^x \\ & + (l_1 i_y + l_3 \bmod N) \mathbf{p}^y \\ & + l_4 \mathbf{m}^x + l_5 \mathbf{m}^y + (l_4 i_y + l_5 i_x + l_6 \bmod N) \mathbf{g}. \end{aligned} \quad (1)$$

Here $(\mathbf{e}, \mathbf{p}^x, \mathbf{p}^y, \mathbf{m}^x, \mathbf{m}^y, \mathbf{g})$ are six distinct Abelian anyon types which generate all of the anyons in the model. An excited a stabilizer on lattice sites $(i_x, i_y) = 0 \bmod N$ corresponds to an ‘‘electric’’ \mathbf{e} excitation, whereas \mathbf{p}^x and \mathbf{p}^y correspond to minimal electric dipoles of excited a stabilizers of x - and y -orientations, respectively. Likewise, the ‘‘magnetic’’ $\mathbf{m}^{x,y}$ excitations correspond to excited $b^{x,y}$ stabilizers on lattice sites $(i_x, i_y) = 0 \bmod N$, while \mathbf{g} is a minimal magnetic dipole. According to (1), stabilizers excited at different sites (i_x, i_y) generally correspond to different types of anyons. The l_1 through l_6 in (1) are \mathbb{Z}_N integers.

The GSD of this model, first worked out for prime N [17] and subsequently for arbitrary N [20], is

$$\text{GSD} = N^3 \text{gcd}(L_x, N) \text{gcd}(L_y, N) \text{gcd}(L_x, L_y, N) \quad (2)$$

for $L_x \times L_y$ torus. Further details of R2TC can be found in the Supplemental Materials (SM) [33]. Kitaev’s toric code by contrast consists of one electric and one magnetic excitation and has the $\text{GSD} = N^2$ irrespective of the lattice size.

There are six Wegner-Wilson (WW) operators W_1 through W_6 , written as a product of X -operators, generating the GSD of R2TC (see [33] for their precise definitions). They represent the creation and annihilation process (CAP) of a y -oriented electric dipole and anti-dipole pair along the x - (W_1) and y -axis (W_2), of an x -oriented electric dipole and anti-dipole pair along the x - (W_3) and y -axis (W_4), and of an electric monopole and anti-monopole along the x - (W_5) and y -axis (W_6).

Another set of six WW operators \widetilde{W}_1 through \widetilde{W}_6 , given as the product of Z -operators [33], represents the CAP of a m^x and anti- m^x monopole pair along the y - (\widetilde{W}_1) and x -axis (\widetilde{W}_2), of an m^y and anti- m^y monopole pair along the y - (\widetilde{W}_3) and x -axis (\widetilde{W}_4), and of an x -oriented m^y -dipole and anti-dipole pair along the y - (\widetilde{W}_5) and x -axis (\widetilde{W}_6). \widetilde{W}_5 and \widetilde{W}_6 also represent the CAP of y -oriented m^x -dipole and anti-dipole pair along the y - and x -axis, respectively. It is a subtle feature of R2TC that x -oriented m_x -dipole and y -oriented m_y dipole are not distinct and should be considered a single type of magnetic dipole [19]. (All the CAPs are graphically represented in SM [33].) Depending on the system size $L_x \times L_y$, some WW operators fail to act as logical operators and create the sensitive dependence of GSD shown in (2) [33].

We can calculate the TEE of R2TC by adapting the method of [34] and writing a ground state as

$$|\psi\rangle = |G|^{-1/2} \sum_{g \in G} g |0\rangle, \quad (3)$$

where $|0\rangle$ is a product state satisfying $Z|0\rangle = |0\rangle$ for all the Z -operators. The group G for R2TC is generated by b_i^x, b_i^y as well as some subset of W_1 through W_6 , all of which are written in terms of X -operators and mutually commuting. A choice of WW operators corresponds to a particular state in the degenerate ground state subspace. [35]

The group cardinality $|G|$ depends on how many WW operators we include besides the b_i^x, b_i^y ’s.

The entanglement entropy of a region A for the ground state $|\psi\rangle$ is obtained after dividing the lattice into two non-overlapping regions A and B , and calculating [33, 34]

$$S_A = \log(|G|/(|G_A| \cdot |G_B|)), \quad (4)$$

where the set G_A (G_B) consists of elements of G that have support exclusively in region A (B). The formula remains valid for both contractible and non-contractible boundaries.

First, we consider the region A in the form of a $l_x \times l_y$ rectangle and find the entropy [33],

$$S_A = [4(l_x + l_y + 1) - 3] \log N, \quad (5)$$

where we used $|\psi\rangle$ in (3) with g generated by (b_i^x, b_i^y) but none of the WW operators. The area law part of the entropy is proportional to $4(l_x + l_y + 1)$ equal to the number of *marginal stabilizers*, referring to those b_i^x, b_i^y stabilizers with support on both A and B - see Fig. 2 (a) for graphical illustration [33]. The important remaining factor is $\gamma = 3 \log N$, which we associate as the TEE of R2TC. It shows no system size dependence, similar to the conclusion on a different topological model [24]. Identical conclusions for S_A and γ are reached if we use G generated with a_i ’s (but none of the \widetilde{W} ’s) [33]. The ordinary \mathbb{Z}_N toric code has $\gamma = \log N$ for the contractible boundary.

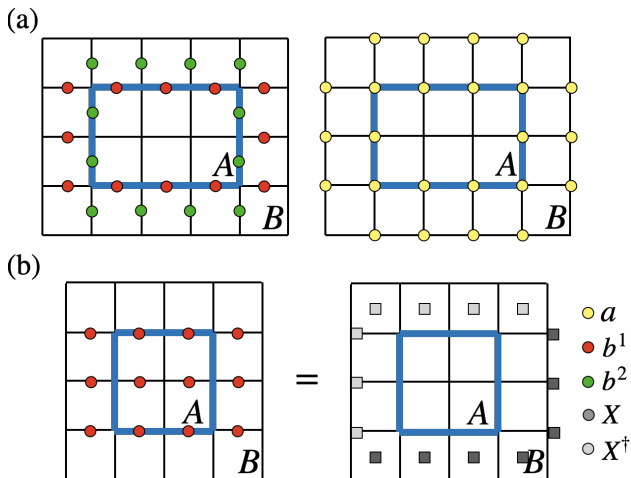


FIG. 2: Region A consists of spins on the blue boundary line and its interior. (a) Marginal stabilizers among b_i^x , b_i^y 's (left) and a_i 's (right) having support in both A and B regions are indicated as colored circles. (b) Product of stabilizers in the region A (left) is equal to the product of X (and X^\dagger) operators along the boundary just outside of A (right).

In further demonstration that the assignment $\gamma = 3 \log N$ is not arbitrary, we show that it is related to three *boundary operators*, defined as

$$\prod_{b_i^x \notin G_B} b_i^x, \quad \prod_{b_i^y \notin G_B} b_i^y, \quad \prod_{b_i^x, b_i^y \notin G_B} (b_i^x)^{-i_y} (b_i^y)^{i_x}. \quad (6)$$

In each case, we have the product of b 's with $i \notin G_B$ meaning that the corresponding stabilizer at $i = (i_x, i_y)$ is not fully supported in region B . This includes stabilizers fully supported in A , and some marginal stabilizers as shown in Fig. 2. Invoking explicit expressions of b_i^x, b_i^y in terms of X (see Fig. 1 and [33]), one finds that all the X -operators in the interior of A cancel out for the three products in (6), leaving only the product of X 's and X^\dagger 's along the boundary ∂A as illustrated in Fig. 2 (b). Formally, the three boundary operators in (6) provide three additional elements to G_B that are not made up of b_i stabilizers lying entirely in the region B . As a result, $|G_B|$ is larger by N^3 than the cardinality without such contributions, and give rise to $\gamma = 3 \log N$ in TEE. To further check the validity of our results, we followed the TEE extraction strategy prescribed in [27] and found $\gamma = 3 \log N$.

So far we have left out the W 's as generators of G . When they are included in G , one can without loss of generality choose to place them entirely in the region B but not in A . This changes the cardinality of both G and G_B but not of G_A , in such a way that the ratio $|G|/|G_B|$ and hence the TEE remains unchanged [33]. The argument fails for the non-contractible boundary since some of the WW operators must cross the boundary no matter how they are deformed. The state constructed in (3) is only one of the possible ground states, but one can show

that all other ground states share the same TEE as long as the boundary is contractible [33].

We now consider a pair of parallel and non-contractible boundaries along the x - or y -axis of the torus and call them x -cut and y -cut, respectively. For non-contractible boundaries, a particular combination of the ground states called the minimum entropy states (MESs), constructed as a simultaneous eigenstate of *all* logical operators running along the cut, plays a significant role in the consideration of TEE [28, 36]. In general, the eigenvalue of any given logical operator is an integer power mod N of ω . It can be shown that in the R2TC, MESs with different eigenvalues of logical operators yield the same TEE [33]. It thus suffices to construct the MES with eigenvalue $+1$ for all the corresponding logical operators, by generating the group G using b_i^1, b_i^2 , and W_1, W_3, W_5 defined along the x -axis. (WW operators defined along the y -axis are W_2, W_4, W_6 .)

Now we are ready to construct a MES for the x -cut as

$$|\psi_{\text{MES}}\rangle = |G_{\text{MES}}|^{-1/2} \sum_{g \in G_{\text{MES}}} g|0\rangle, \quad (7)$$

with the group G_{MES} generated by b_i^x, b_i^y , and W_1, W_3, W_5 . First of all, note that a state in (7) is automatically an eigenstate of $g \in G_{\text{MES}}$ with eigenvalue $+1$ and thus of W_1, W_3, W_5 . It is also an eigenstate of all \tilde{W} 's running along the x -axis, with eigenvalue $+1$, as they commute with (W_1, W_3, W_5) [33]. Therefore, $|\psi_{\text{MES}}\rangle$ constructed in (7) is a MES for arbitrary $L_x \times L_y$. The entanglement entropy of such MES can be obtained [33], $S_{\text{MES}}^x = 4L_x \log N - \gamma_{\text{MES}}^x$, with

$$\gamma_{\text{MES}}^x = \log(N^4 \gcd(L_x, N)^2). \quad (8)$$

A similar construction of MES for the y -cut uses (W_2, W_4, W_6) as generators and gives

$$\gamma_{\text{MES}}^y = \log(N^4 \gcd(L_y, N)^2). \quad (9)$$

We have successfully confirmed that the system size dependence not only exists in GSD [17, 20] but also in TEE for the bi-partition by *non-contractible* loops. Having explicit formulas for both TEE in (8)-(9) and GSD in (2), we now look for a theoretical framework to understand them.

The \mathbb{Z}_N R2TC has translation symmetry in both the x and y directions. However, acting on an anyon with translation symmetry will, in general, change the anyon type as demonstrated by (1). For example, an anyon with $l_1 = 1$ and all other $l_i = 0$ on the site $(0, 0)$ transforms under translation symmetry T_x to an anyon with $l_1 = 1$ but $l_2 = -1$ on site $(1, 0)$, and is therefore topologically distinct from the original anyon. It also follows from (1) that both T_x and T_y generate anyon permutations of rank N , that is, T_x^N and T_y^N leave the anyon type unchanged. If we coarse-grain to an $N \times N$ unit cell, then we can roughly think of the system as having an ‘‘on-site’’ symmetry group $G = \mathbb{Z}_N^{(x)} \times \mathbb{Z}_N^{(y)}$ (the superscript notation is just a reminder that T_x generates

the first copy of \mathbb{Z}_N and T_y the second). Although the symmetry is not actually on-site, we will treat it as such in what follows according to the crystalline equivalence principle [37]. In this view, the R2TC should be viewed as a $\mathbb{Z}_N \times \mathbb{Z}_N$ SET.

In this coarse-grained view, choosing a linear system size L_x such that N does not divide L_x introduces a *symmetry defect* piercing the x handle of the torus. This means that, if we define

$$L_x \bmod N \equiv m, \quad L_y \bmod N \equiv n, \quad (10)$$

any excitation traversing the x handle of the torus will be acted upon by the element $\mathbf{g} = m$ of $\mathbb{Z}_N^{(x)}$ (in additive notation). Similarly, L_y not divisible by N gives rise to another symmetry defect $\mathbf{h} = n$ of $\mathbb{Z}_N^{(y)}$ piercing the y handle of the torus. Any excitation that traverses the y handle of the torus will be acted on by \mathbf{h} .

It is well-understood how to characterize symmetry defects in the presence of anyons; the correct mathematical framework is a ‘‘G-crossed modular tensor category.’’ [10, 11, 31, 32] (To avoid confusion with the notation G for the group of generators earlier, we use the roman G when referring to symmetry defects.) We briefly summarize the salient results of [10]. Given a G-enriched topological phase, there are many symmetry defects associated to a group element $\mathbf{g} \in G$; we call the set of such defects $\mathcal{C}_{\mathbf{g}}$. We denote one such defect as $a_{\mathbf{g}}$. (If $\mathbf{0}$ is the identity element of G , then the set of $\mathbf{0}$ defects is just the anyons of the theory.) Any one of the defects associated to \mathbf{g} can be obtained from any other by fusing it with some anyon.

Each symmetry defect $a_{\mathbf{g}}$ has essentially the same properties as an anyon, including all the data associated with fusion and braiding. The main difference is that if one defect braids around another, it can change defect type because it is acted upon by an element of the symmetry group. In particular, if $a_{\mathbf{g}}$ does a full braid with $b_{\mathbf{h}}$ ($\mathbf{h} \in G$), then we say that $a_{\mathbf{g}}$ transforms as $a_{\mathbf{g}} \rightarrow {}^{\mathbf{h}}a_{\mathbf{g}}$. If it turns out that ${}^{\mathbf{h}}a_{\mathbf{g}} = a_{\mathbf{g}}$, that is, the defect type does not change under the action of \mathbf{h} , then we say that $a_{\mathbf{g}}$ is \mathbf{h} -invariant. We denote the set of \mathbf{h} -invariant \mathbf{g} defects by $\mathcal{C}_{\mathbf{g}}^{\mathbf{h}}$.

The number of distinct \mathbf{g} defects (denoted $|\mathcal{C}_{\mathbf{g}}|$) is

$$|\mathcal{C}_{\mathbf{g}}| = |\mathcal{C}_{\mathbf{0}}^{\mathbf{g}}| = \# \text{ of } \mathbf{g}\text{-invariant anyons.} \quad (11)$$

It is straightforward to show that if all the anyons are Abelian, then all \mathbf{g} defects have the same quantum dimension. Using the fact that the total quantum dimension of the \mathbf{g} defects must equal the total quantum dimension of the anyons, it follows that the quantum dimension $d_{a_{\mathbf{g}}}$ of any \mathbf{g} defect is

$$d_{a_{\mathbf{g}}} = \sqrt{\frac{\# \text{ of anyons}}{\# \text{ of } \mathbf{g}\text{-invariant anyons}}}. \quad (12)$$

For the contractible boundary, TEE of a state with a

quasiparticle a inside the region A is [27, 36]

$$\gamma = \log \frac{\mathcal{D}}{d_a}. \quad (13)$$

In the ground state for L_x, L_y divisible by N , there are no quasiparticle inside A (other than the vacuum itself) and $\gamma = \log \mathcal{D} = 3 \log N$. An arbitrary L_x, L_y means that defects \mathbf{g} and \mathbf{h} are piercing the x and y handles of the torus, respectively. Therefore, still only the vacuum is inside A , which means $\gamma = 3 \log N$, in agreement with our earlier result, (5). We see that the defect picture gives a consistent interpretation of the lack of system size dependence in the case of contractible boundary.

In the absence of symmetry defects, the entanglement entropy of a MES on the torus associated to an anyon $a_{\mathbf{0}}$ threading the x -cut cycle is given by [28, 36]

$$\gamma_{\text{MES}}^{(a_{\mathbf{0}})} = 2 \log \frac{\mathcal{D}}{d_{a_{\mathbf{0}}}}. \quad (14)$$

We assume that the analogous formula holds in twisted sectors, i.e., when a symmetry defect $a_{\mathbf{g}}$ threads the x -cut cycle instead:

$$\gamma_{\text{MES}}^{(a_{\mathbf{g}})} = 2 \log \frac{\mathcal{D}}{d_{a_{\mathbf{g}}}}. \quad (15)$$

Ref. [38] found that various other TEE formulas involving only anyons, such as Eq. (13), can be directly generalized to the defect case in the same way, which justifies our assumption. When all the anyons are Abelian, \mathcal{D}^2 is just the total number of anyons, so we find

$$\gamma_{\text{MES}}^{(a_{\mathbf{g}})} = \log (\# \text{ of } \mathbf{g}\text{-invariant anyons}) \quad (16)$$

One can explicitly show that indeed, the number of \mathbf{g} -invariant anyons in the R2TC is $N^4 \gcd(L_x, N)^2$ [33], in agreement with γ_{MES}^x in (8). A similar reasoning of $\gamma_{\text{MES}}^{(a_{\mathbf{h}})}$ correctly captures γ_{MES}^y in (9).

We conclude that the system size dependence of the TEE can be adequately explained by thinking of the system as a coarse-grained system enriched by a $\mathbb{Z}_N \times \mathbb{Z}_N$ symmetry arising from microscopic translations.

Likewise, the torus GSD can be explained in the same language. G-crossed modularity [10] requires that

$$\begin{aligned} \text{GSD}(\mathbf{g}, \mathbf{h}) &= \# \text{ of } \mathbf{g}\text{-invariant } \mathbf{h} \text{ defects} \\ &= \# \text{ of } \mathbf{h}\text{-invariant } \mathbf{g} \text{ defects} \end{aligned} \quad (17)$$

(Unlike our TEE formula, this formula has been proven rigorously.) For $\mathbf{g} = 0$, this is just the number of \mathbf{h} defects, which, as already stated, is $N^4 \gcd(L_y, N)^2$, with an analogous formula when the roles of L_x and L_y swap. We carefully show in the SI [33] that the general formula is [33]

$$\begin{aligned} &\# \text{ of } \mathbf{g}\text{-invariant } \mathbf{h} \text{ defects} \\ &= N^3 \gcd(L_x, N) \gcd(L_y, N) \gcd(L_x, L_y, N) \end{aligned} \quad (18)$$

which matches the GSD formula in (2).

We have demonstrated that both the TEE and GSD of the R2TC can be comprehensively understood by conceptualizing it as a translation SET and using the symmetry defect theory.

A few additional remarks are in order. One can use the tensor network ground state wave function for R2TC proposed in [19] to compute the entanglement entropy numerically. Due to severe computational costs, it turns out the calculation is currently limited to $N = 2$ and $L_y \leq 3$ for the case of the y -cut, with $L_x \leq 5$. Following the procedure outlined in [19, 33, 39], we numerically find the entanglement entropy in excellent agreement with $S_{\text{MES}}^y = 4L_y \log N - \log(N^4 \text{gcd}(L_y, N)^2)$ for $N = 2$, $L_y = 3$ and $L_x = 4, 5$, confirming the validity of our derivation. Secondly, it is known that spurious TEE can appear for some non-topological states [25, 40, 41]. To check that our results are not being plagued by such effects, we use the model proposed in [41] and construct bulk products similar to (6). After the interior terms again cancel out, leaving the product of operators along the boundary of A . Importantly, this product does not completely encircle the boundary, as is the case in R2TC and other topological models, but is limited to a finite segment. Consequently, the TEE depends on the shape of the boundary and the area of the region (see Fig. S3). With this observation, we can ensure that the TEE of R2TC is a genuine TEE. This comprehension can serve as a useful diagnostic for distinguishing between spurious and genuine TEE.

In conclusion, we have performed systematic calculations of TEE for the rank-2 toric code and found system size dependence similar to the system size dependence of the GSD. We quantitatively explain the TEE

by viewing the R2TC as a translation SET with symmetry defects threaded through non-contractible cycles of the torus. Our work shows that the symmetry defect picture is powerful enough to straightforwardly predict topological properties beyond the GSD while not requiring a distinction between local and global equivalence of excitation configurations. Given the wide range of unique features in such translation SETs, it would be highly interesting to realize such models in spin, Rydberg atom, or other synthetic systems. It may also be possible to use our understanding of such translation SETs in (2+1) dimensions as a stepping stone to a more general understanding of (3+1)-dimensional phases with system size-dependent GSDs, including translation SETs and fracton topological orders.

Acknowledgments. - We are grateful to Isaac Kim for helpful discussions and feedback, and to Yizhi You for an earlier collaboration. Y.-T. O. acknowledges support from the National Research Foundation of Korea (NRF), funded by the Korean government (MSIT), under grants No. RS-2023-00220471 and NRF-2022R1I1A1A01065149, as well as from the Basic Science Research Program funded by the Ministry of Education under grant 2014R1A6A1030732. D.B. was supported for part of this work by the Simons Collaboration on Ultra-Quantum Matter, which is a grant from the Simons Foundation (No. 651440). J.H.H. was supported by the National Research Foundation of Korea (NRF) grant funded by the Korea government (MSIT) (No. 2023R1A2C1002644). He acknowledges KITP, supported in part by the National Science Foundation under Grant No. NSF PHY-1748958, where this work was finalized.

-
- [1] X.-G. Wen, *Quantum Field Theory of Many-Body Systems: From the Origin of Sound to an Origin of Light and Electrons* (Oxford University Press, 2007).
 - [2] A. Kitaev, *Annals of Physics* **303**, 2 (2003).
 - [3] X.-G. Wen, *Phys. Rev. B* **65**, 165113 (2002).
 - [4] S.-P. Kou and X.-G. Wen, *Phys. Rev. B* **80**, 224406 (2009).
 - [5] A. M. Essin and M. Hermele, *Phys. Rev. B* **87**, 104406 (2013).
 - [6] A. Mesaros and Y. Ran, *Phys. Rev. B* **87**, 155115 (2013).
 - [7] D. T. Stephen, J. Garre-Rubio, A. Dua, and D. J. Williamson, *Phys. Rev. Res.* **2**, 033331 (2020).
 - [8] Y.-M. Lu and A. Vishwanath, *Phys. Rev. B* **93**, 155121 (2016).
 - [9] X. Chen, *Reviews in Physics* **2**, 3 (2017).
 - [10] M. Barkeshli, P. Bonderson, M. Cheng, and Z. Wang, *Phys. Rev. B* **100**, 115147 (2019).
 - [11] N. Tarantino, N. H. Lindner, and L. Fidkowski, *New Journal of Physics* **18**, 035006 (2016).
 - [12] X.-G. Wen, *Phys. Rev. Lett.* **90**, 016803 (2003).
 - [13] Y.-Z. You and X.-G. Wen, *Phys. Rev. B* **86**, 161107 (2012).
 - [14] P. Gorantla, H. T. Lam, N. Seiberg, and S.-H. Shao, *Phys. Rev. B* **104**, 235116 (2021).
 - [15] P. Gorantla, H. T. Lam, N. Seiberg, and S.-H. Shao, *Phys. Rev. B* **106**, 045112 (2022).
 - [16] P. Gorantla, H. T. Lam, N. Seiberg, and S.-H. Shao, *Phys. Rev. B* **108**, 075106 (2023).
 - [17] Y.-T. Oh, J. Kim, E.-G. Moon, and J. H. Han, *Phys. Rev. B* **105**, 045128 (2022).
 - [18] Y.-T. Oh, J. Kim, and J. H. Han, *Phys. Rev. B* **106**, 155150 (2022).
 - [19] Y.-T. Oh, S. D. Pace, J. H. Han, Y. You, and H.-Y. Lee, *Phys. Rev. B* **107**, 155151 (2023).
 - [20] S. D. Pace and X.-G. Wen, *Phys. Rev. B* **106**, 045145 (2022).
 - [21] G. Delfino, W. B. Fontana, P. R. S. Gomes, and C. Chamon, *SciPost Phys.* **14**, 002 (2023).
 - [22] G. Delfino, C. Chamon, and Y. You, “2d fractons from gauging exponential symmetries,” (2023), [arXiv:2306.17121](https://arxiv.org/abs/2306.17121) [cond-mat.str-el].
 - [23] H. Ebisu, *Phys. Rev. B* **107**, 125154 (2023).
 - [24] H. Ebisu, “Entanglement entropy of higher rank topological phases,” (2023), [arXiv:2302.11468](https://arxiv.org/abs/2302.11468) [cond-mat.str-el].

- [25] H. Watanabe, M. Cheng, and Y. Fuji, *Journal of Mathematical Physics* **64**, 051901 (2023).
- [26] M. Levin and X.-G. Wen, *Phys. Rev. Lett.* **96**, 110405 (2006).
- [27] A. Kitaev and J. Preskill, *Phys. Rev. Lett.* **96**, 110404 (2006).
- [28] Y. Zhang, T. Grover, A. Turner, M. Oshikawa, and A. Vishwanath, *Phys. Rev. B* **85**, 235151 (2012).
- [29] J. C. Teo, T. L. Hughes, and E. Fradkin, *Annals of Physics* **360**, 349 (2015).
- [30] D. Bulmash and M. Barkeshli, *Phys. Rev. B* **97**, 235112 (2018).
- [31] V. Turaev, “Homotopy field theory in dimension 3 and crossed group-categories,” (2000), [arXiv:math/0005291 \[math.GT\]](https://arxiv.org/abs/math/0005291).
- [32] P. Etingof, D. Nikshych, and V. Ostrik, *Quantum Topology* **1**, 209 (2010), [arXiv:0909.3140](https://arxiv.org/abs/0909.3140).
- [33] See the supplemental material for details.
- [34] A. Hamma, R. Ionicioiu, and P. Zanardi, *Phys. Rev. A* **71**, 022315 (2005).
- [35] Starting from a product state in the X basis, one can alternatively construct the group G from a_i and the associated WW operators in the Z -basis. This results in added complexity since WW operators in the Z -basis do not always span the entire ground states. For this reason we employ, without loss of generality, the construction of $|\psi\rangle$ in the X -basis for the calculation of entanglement entropy.
- [36] S. Dong, E. Fradkin, R. G. Leigh, and S. Nowling, *Journal of High Energy Physics* **2008**, 016 (2008).
- [37] R. Thorngren and D. V. Else, *Phys. Rev. X* **8**, 011040 (2018).
- [38] B.-B. Chen, H.-H. Tu, Z. Y. Meng, and M. Cheng, *Phys. Rev. B* **106**, 094415 (2022).
- [39] J. I. Cirac, D. Poilblanc, N. Schuch, and F. Verstraete, *Phys. Rev. B* **83**, 245134 (2011).
- [40] L. Zou and J. Haah, *Phys. Rev. B* **94**, 075151 (2016).
- [41] D. J. Williamson, A. Dua, and M. Cheng, *Phys. Rev. Lett.* **122**, 140506 (2019).

Supplementary Information for ‘‘Unveiling UV/IR Mixing Via Symmetry Defects: A View from Topological Entanglement Entropy’’

Jintae Kim^{1,*}, Yun-Tak Oh,² Daniel Bulmash,^{3,4} and Jung Hoon Han^{1,†}

¹*Department of Physics, Sungkyunkwan University, Suwon 16419, South Korea*

²*Division of Display and Semiconductor Physics, Korea University, Sejong 30019, Korea*

³*Department of Physics, United States Naval Academy, Annapolis, MD 21402, USA*

⁴*Department of Physics and Center for Theory of Quantum Matter, University of Colorado Boulder, Boulder, Colorado 80309, USA*

(Dated: October 17, 2023)

I. ENTANGLEMENT ENTROPY FORMULA

In this section, we summarize a derivation of the entanglement entropy expression presented in (4) [24, 34]. The entanglement entropy S_A associated with the region A is formally defined as

$$S_A = \lim_{n \rightarrow 1} \frac{1}{1-n} \log \text{Tr}[\rho_A^n], \quad (\text{S1})$$

where $\rho_A = \text{Tr}_B[\rho]$ is the reduced density matrix for region A . S_A is also recognized as the Renyi entanglement entropy. Starting from the pure state expression in (3), ρ_A can be expressed as

$$\begin{aligned} \rho_A &= \text{Tr}_B[|\psi\rangle\langle\psi|] \\ &= |G|^{-1} \text{Tr}_B \left[\sum_{g \in G, g' \in G} g |0\rangle\langle 0| (gg')^\dagger \right] \\ &= |G|^{-1} \text{Tr}_B \left[\sum_{g \in G, g' \in G} g_A |0\rangle_A \langle 0|_A (g_A g'_A)^\dagger \otimes g_B |0\rangle_B \langle 0|_B (g_B g'_B)^\dagger \right] \\ &= |G|^{-1} \sum_{i,j,g \in G, g' \in G} g_A |0\rangle_A \langle 0|_A (g_A g'_A)^\dagger \otimes \langle 0|_B (g_B g'_B)^\dagger g_B |0\rangle_B, \end{aligned} \quad (\text{S2})$$

where $g = g_A \otimes g_B$ and $|0\rangle = |0\rangle_A \otimes |0\rangle_B$. The requisite condition for the non-vanishing of $\langle 0|_B (g_B g'_B)^\dagger g_B |0\rangle_B$ is $g'_B = I_B$. Subsequently, the formulation for ρ_A adopts the structure

$$\rho_A = |G|^{-1} \sum_{g \in G, g' \in G_A} g_A |0\rangle_A \langle 0|_A (g_A g'_A)^\dagger, \quad (\text{S3})$$

where $G_A = \{g \in G | g = g_A \otimes I_B\}$. Employing (S3), we proceed to deduce $\rho_A^2 = |G_A||G_B|/|G|\rho_A$ [24, 34]. After all, we arrive at

$$\begin{aligned} S_A &= \lim_{n \rightarrow 1} \frac{1}{1-n} \log \text{Tr} \left[\left(\frac{|G_A||G_B|}{|G|} \right)^{n-1} \rho_A \right] \\ &= \log \left(\frac{|G|}{|G_A| \cdot |G_B|} \right) \end{aligned} \quad (\text{S4})$$

as the conclusive expression.

II. STABILIZER IDENTITIES IN R2TC

In the rank-2 toric code (R2TC), there are three stabilizers a_i , b_i^x , and b_i^y associated with sites i , links $(i, i + \hat{x})$, and $(i, i + \hat{y})$ on a square lattice, respectively. They correspond to one electric and two magnetic excitations as:

$$\begin{aligned} a_i &= Z_{0,i} Z_{0,i-\hat{x}}^{-1} Z_{0,i-\hat{y}}^{-1} Z_{0,i-\hat{x}-\hat{y}} Z_{2,i-\hat{y}} Z_{2,i}^{-2} Z_{2,i+\hat{y}} Z_{1,i-\hat{x}} Z_{1,i}^{-2} Z_{1,i+\hat{x}} \\ b_i^x &= X_{2,i}^1 X_{2,i+\hat{x}}^{-1} X_{0,i} X_{0,i-\hat{y}}^{-1} \\ b_i^y &= X_{1,i} X_{1,i+\hat{y}}^{-1} X_{0,i} X_{0,i-\hat{x}}^{-1}. \end{aligned} \quad (\text{S5})$$

We label the sites by $i = (i_x, i_y)$. \mathbb{Z}_N Pauli- X, Z operators are defined by their actions ($\omega = e^{2\pi i/N}$):

$$X_{a,i}|g\rangle_{a,i} = |g+1 \pmod{N}\rangle_{a,i}, \quad Z_{a,i}|g\rangle = \omega^g|g\rangle_{a,i}. \quad (\text{S6})$$

Operators with subscript 0 are defined at the center of the plaquette associated with the site i while those with subscripts 1, 2 are both defined at the site as illustrated in Fig. 1.

We summarize several identities held by stabilizers and logical operators of R2TC that will prove to be of use in the evaluation of TEE. Three of them come directly from the definition of stabilizers:

$$I_1 \equiv \prod_i a_i = 1 \quad I_2 \equiv \prod_i b_i^x = 1 \quad I_3 \equiv \prod_i b_i^y = 1. \quad (\text{S7})$$

The product \prod_i runs over all the sites of the square lattice forming a torus, $1 \leq i_x \leq L_x$, $1 \leq i_y \leq L_y$. Heuristically, they imply the conservation of the total electric (I_1) and two magnetic (I_2, I_3) charges mod \mathbb{Z}_N . The other three identities are

$$\begin{aligned} I_4 &\equiv \left[\prod_i (a_i)^{i_x} \right]^{c_x} = 1, \\ I_5 &\equiv \left[\prod_i (a_i)^{i_y} \right]^{c_y} = 1, \\ I_6 &\equiv \left[\prod_i (b_i^x)^{-i_y} (b_i^y)^{i_x} \right]^{c_{xy}} = 1. \end{aligned} \quad (\text{S8})$$

Each stabilizer is raised to a power of the coordinate, and the identities I_4, I_5, I_6 refer to the conservation of electric dipoles in the x direction, electric dipoles in the y direction, and magnetic angular momentum, respectively. Importantly, the identities are obtained when the products are raised to appropriate ‘‘winding numbers’’ c_x, c_y, c_{xy} given by

$$\begin{aligned} c_x &= N/\text{gcd}(L_x, N) = \text{lcm}(L_x, N)/L_x, \\ c_y &= N/\text{gcd}(L_y, N) = \text{lcm}(L_y, N)/L_y, \\ c_{xy} &= N/\text{gcd}(L_x, L_y, N). \end{aligned} \quad (\text{S9})$$

The necessity to introduce them becomes clear when we evaluate

$$\begin{aligned} \prod_i (a_i)^{i_x} &= \prod_{i_y} Z_{1, \hat{x}+i_y \hat{y}}^{L_x} Z_{1, L_x \hat{x}+i_y \hat{y}}^{-L_x} \\ \prod_i (a_i)^{i_y} &= \prod_{i_x} Z_{2, i_x \hat{x}+\hat{y}}^{L_y} Z_{2, i_x \hat{x}+L_y \hat{y}}^{-L_y} \\ \prod_i (b_i^x)^{-i_y} (b_i^y)^{i_x} &= \prod_{i_y} X_{0, L_x \hat{x}+i_y \hat{y}}^{L_x} \prod_{i_x} X_{0, i_x \hat{x}+L_y \hat{y}}^{-L_y}. \end{aligned} \quad (\text{S10})$$

In general they are not equal to an identity unless L_x, L_y are multiples of N . To guarantee their identity we need to find the smallest positive integers n_x, n_y , and n_{xy} satisfying

$$\begin{aligned} L_x n_x \pmod{N} &= 0, \quad L_y n_y \pmod{N} = 0 \\ L_x n_{xy} \pmod{N} &= 0 \quad \& \quad L_y n_{xy} \pmod{N} = 0. \end{aligned} \quad (\text{S11})$$

The first two relations give $n_x = c_x$ and $n_y = c_y$. For n_{xy} ,

$$n_{xy} = \text{lcm} \left(\frac{N}{\text{gcd}(L_x, N)}, \frac{N}{\text{gcd}(L_y, N)} \right) = \frac{N}{\text{gcd}(\text{gcd}(L_x, N), \text{gcd}(L_y, N))} = \frac{N}{\text{gcd}(L_x, L_y, N)} = c_{xy}. \quad (\text{S12})$$

We refer to the six identities I_1 through I_6 as the ‘‘stabilizer identities’’ of the R2TC.

The six stabilizer identities derived above can be used to evaluate the ground state degeneracy (GSD), by comparing the number of identities against the total number of stabilizers in the model. This approach, already used in Kitaev’s toric code paper [2], was applied for the initial GSD calculation of \mathbb{Z}_N R2TC [17] assuming N is a prime number.

We now have relaxed this condition and obtained identities (S7) and (S8) that hold for arbitrary integer N . Each of the three identities I_1, I_2, I_3 generates N constraint for the stabilizers since $(I_1)^{n_1} = (I_2)^{n_2} = (I_3)^{n_3} = 1$ for $1 \leq n_1, n_2, n_3 \leq N$. The GSD becomes $N \times N \times N = N^3$. From the three remaining identities we have $(I_\alpha)^{n_\alpha} = 1$ with $1 \leq n_4 \leq \gcd(L_x, N)$, $1 \leq n_5 \leq \gcd(L_y, N)$, and $1 \leq n_6 \leq \gcd(L_x, L_y, N)$, respectively. The full GSD formula of (2) is recovered in this simple manner.

Among the six identities, $\{I_2, I_3, I_6\}$ come from taking the product of magnetic stabilizers and the remaining $\{I_1, I_4, I_5\}$ from those of electric stabilizers. The fact that there are three identities for each type of stabilizers plays a crucial role in the evaluation of TEE.

III. WW OPERATORS IN X -OPERATOR BASIS

There are six Wegner-Wilson (WW) operators, which are products of X 's. These operators correspond to the movement of electric monopoles and dipoles along the non-contractible loops of the torus [19]:

$$\begin{aligned} W_{1,i_y} &= \prod_{i_x=1}^{L_x} X_{0,i}, & W_{2,i_x} &= \prod_{i_y=1}^{L_y} X_{2,i}, & W_{3,i_y} &= \prod_{i_x=1}^{L_x} X_{1,i}, & W_{4,i_x} &= \prod_{i_y=1}^{L_y} X_{0,i} \\ W_{5,i_y} &= \prod_{i_x=1}^{\text{lcm}(L_x,N)} (X_{1,i})^{i_x} (X_{0,i})^{i_y}, & W_{6,i_x} &= \prod_{i_y=1}^{\text{lcm}(L_y,N)} (X_{2,i})^{i_y} (X_{0,i})^{i_x}. \end{aligned} \quad (\text{S13})$$

In some cases, i_x and i_y can be omitted for simplicity. An arbitrary WW operator $W_{a,i'_x(i'_y)}$ can be expressed as the product of WW operators in Eq. (S13) and the stabilizers b_i^x and b_i^y .

The WW operators can be used to account for the GSD. Among the six WW operators, W_2 and W_3 satisfy $(W_2)^N = (W_3)^N = 1$, each giving a factor N for the number of independent logical operators and therefore the distinct ground states. With W_5 and W_6 the degeneracy count is not as simple, since we do not have $(W_5)^{\gcd(L_x,N)}$ and $(W_6)^{\gcd(L_y,N)}$ equal to unity in general. Instead, we can show that W_5 and W_6 can be re-organized as

$$\begin{aligned} W_5 &= \prod_{i_x=1}^{L_x} X_{1,i}^{\frac{\text{lcm}(L_x,N)}{2L_x} \left(\frac{\text{lcm}(L_x,N)}{L_x} - 1 \right) + \frac{\text{lcm}(L_x,N)}{L_x} i_x} X_{0,i}^{\frac{\text{lcm}(L_x,N)}{L_x} i_y} \\ W_6 &= \prod_{i_y=1}^{L_y} X_{2,i}^{\frac{\text{lcm}(L_y,N)}{2L_y} \left(\frac{\text{lcm}(L_y,N)}{L_y} - 1 \right) + \frac{\text{lcm}(L_y,N)}{L_y} i_y} X_{0,i}^{\frac{\text{lcm}(L_y,N)}{L_y} i_x}, \end{aligned} \quad (\text{S14})$$

since the exponents of the $X_{1,i}$, $X_{2,i}$ are $\sum_j (j * L_x + i_x)$ while the one of the $X_{0,i}$ is $\sum_j i_x$. Therefore,

$$\begin{aligned} (W_5)^{\gcd(L_x,N)} &= \prod_{i_x=1}^{L_x} X_{1,i}^{\frac{N}{2} \left(\frac{\text{lcm}(L_x,N)}{L_x} - 1 \right)} = (W_3)^{\frac{N}{2} \left(\frac{\text{lcm}(L_x,N)}{L_x} - 1 \right)} \\ (W_6)^{\gcd(L_y,N)} &= \prod_{i_y=1}^{L_y} X_{2,i}^{\frac{N}{2} \left(\frac{\text{lcm}(L_y,N)}{L_y} - 1 \right)} = (W_2)^{\frac{N}{2} \left(\frac{\text{lcm}(L_y,N)}{L_y} - 1 \right)}, \end{aligned} \quad (\text{S15})$$

both of which are equal to some powers of existing logical operators. Although intuitively clear, one can prove that the two exponents appearing on the r.h.s. are indeed integers. First for N even, the exponents appearing at the far right are obviously integers. For odd N , one can show that $\text{lcm}(L_x, N)/L_x$ is an odd integer, and the exponent is again an integer. (The proof is elementary. When $\text{lcm}(L_x, N)$ and L_x are factorized in terms of prime numbers, both factorizations must contain the same number of 2's in them because N is odd. Hence, the ratio $\text{lcm}(L_x, N)/L_x$ must be expressed as a product of odd prime numbers and become an odd number.) To conclude, $(W_5)^{\gcd(L_x,N)}$ and $(W_6)^{\gcd(L_y,N)}$ are some integer multiples of existing logical operators W_2 and W_3 and no longer independent logical operators.

Finally we come to W_1, W_4 , both of which are products of X_0 's. As the combination $W_1^{n_1} W_4^{n_4}$ with various equivalence relations

$$(n_1, n_4) \equiv (n_1 + N_y, n_4) \equiv (n_1, n_4 + N_x) \equiv (n_1 + L_y, n_4 - L_x) \quad (\text{S16})$$

where $N_x = \gcd(c_y L_x, N)$, $N_y = \gcd(c_x L_y, N)$ [19]. We need to check how many inequivalent integers (n_1, n_4) are allowed under the equivalence relations. Due to the first two relations in (S16), we conclude $1 \leq n_1 \leq N_y$ and

$1 \leq n_4 \leq N_x$. Furthermore, the number of different integer expressions (n_1, n_4) that become equivalent due to $(n_1, n_4) \equiv (n_1 + L_y, n_4 - L_x)$ is

$$\text{lcm}\left(\frac{\text{lcm}(L_x, N_x)}{L_x}, \frac{\text{lcm}(L_y, N_y)}{L_y}\right). \quad (\text{S17})$$

Therefore the total number of independent products of W_1 and W_4 is

$$\begin{aligned} \frac{N_x N_y}{\text{lcm}\left(\frac{\text{lcm}(L_x, N_x)}{L_x}, \frac{\text{lcm}(L_y, N_y)}{L_y}\right)} &= \text{gcd}\left(N_y \text{gcd}(L_x, N_x), N_x \text{gcd}(L_y, N_y)\right) \\ &= N \text{gcd}\left(\text{gcd}(L_x, N), \text{gcd}(L_y, N)\right) \\ &= N \text{gcd}(L_x, L_y, N). \end{aligned} \quad (\text{S18})$$

To conclude, we have degeneracy factors of N from W_2 and W_3 each, $\text{gcd}(L_x, N)$ and $\text{gcd}(L_y, N)$ from W_5 and W_6 each, and the factor of $N \text{gcd}(L_x, L_y, N)$ from the combination of W_1 and W_4 for a total of $N^3 \text{gcd}(L_x, N) \text{gcd}(L_y, N) \text{gcd}(L_x, L_y, N)$ independent logical operators.

For the last, we determine how many WW operators are defined along the x -axis or y -axis to construct the MES. We can be sure that W_3 and W_5 are defined along x -axis, and W_2 and W_6 are defined along y -axis. However, it is tricky to count the numbers of W_1 and W_4 because of equivalence relations in Eq. (S16). When N is a prime number, the following four cases can be observed: (1) both L_x and L_y are multiples of N , (2) only L_x is a multiple of N , (3) only L_y is a multiple of N , and (4) neither L_x nor L_y is a multiple of N . Within each of these cases, the corresponding outcomes are as follows: for case (1), both W_1 and W_4 are present; for case (2), only W_4 is present; for case (3), only W_1 is present; and for case (4), either W_1 or W_4 may exist, which means W_1 and W_4 become identical [17]. The results are summarized in the Table I.

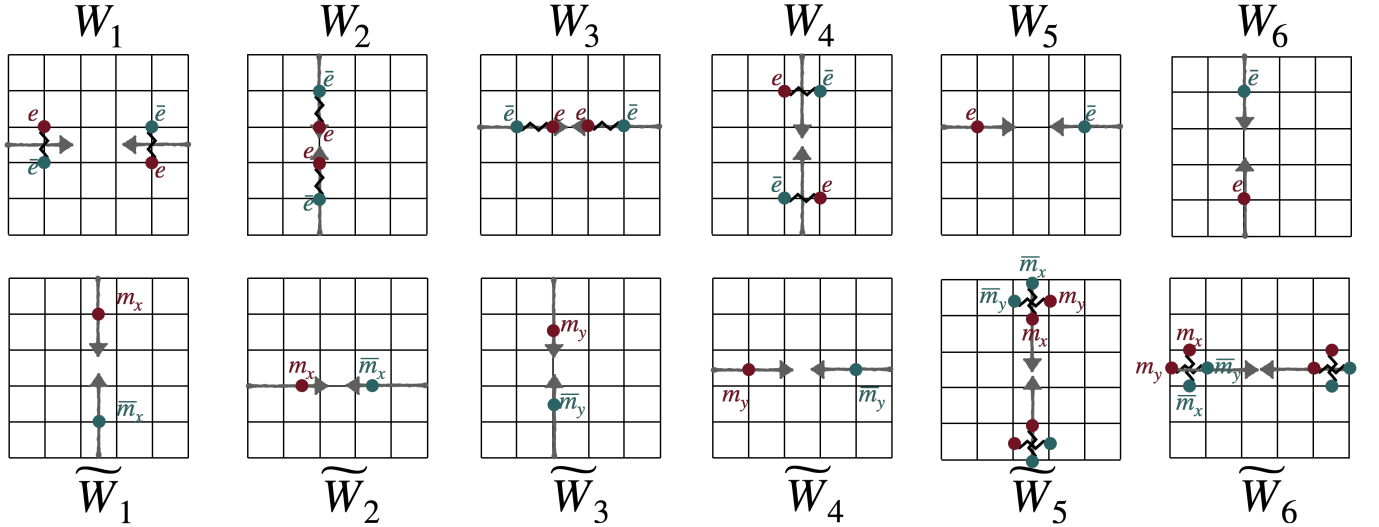


FIG. S1: The CAPs associated with anyons and their corresponding anti-anyon pairs are illustrated for the respective WW operators.

	$L_x \bmod N = 0$	$L_x \bmod N \neq 0$
$L_y \bmod N = 0$	$(W_1 \widetilde{W}_2 W_3 \widetilde{W}_4 W_5 \widetilde{W}_6)$	$(W_1 \widetilde{W}_2 W_3 \widetilde{W}_6)$
	$(\widetilde{W}_1 W_2 \widetilde{W}_3 W_4 \widetilde{W}_5 W_6)$	$(\widetilde{W}_1 W_2 \widetilde{W}_3 W_6)$
$L_y \bmod N \neq 0$	$(\widetilde{W}_2 W_3 \widetilde{W}_4 W_5)$	$(\widetilde{W}_2 W_3)$
	$(W_2 \widetilde{W}_3 W_4 \widetilde{W}_5)$	$(W_{[1 \simeq 4]}, \widetilde{W}_{[1 \simeq 4]})$ $(W_2 \widetilde{W}_3)$

TABLE I: Classification of WW operators that function as logical operators. For each case, upper (lower) sets are the WW operators defined as products along the x - (y -)axis. We assume N is a prime number. The middle row of the final entry ($L_x, L_y \bmod N \neq 0$) shows two WW operators $W_{[1 \simeq 4]}$ and $\widetilde{W}_{[1 \simeq 4]}$, which are neither extended along x or y -direction.

IV. WW OPERATORS IN Z -OPERATOR BASIS

There are six WW operators in terms of Z 's:

$$\begin{aligned}
\widetilde{W}_1 &= \prod_{i_y=1}^{\text{lcm}(L_y, N)} Z_{0, i-\hat{y}} (Z_{1, i} Z_{1, i+\hat{x}}^{-1})^{i_y}, & \widetilde{W}_2 &= \prod_{i_x=1}^{L_x} Z_{2, i} (Z_{2, i} Z_{2, i+\hat{y}}^{-1})^{i_y}, \\
\widetilde{W}_3 &= \prod_{i_y=1}^{L_y} Z_{1, i} (Z_1(\vec{v}_i) Z_1(\vec{v}_i + \hat{x})^{-1})^{i_x}, & \widetilde{W}_4 &= \prod_{i_x=1}^{\text{lcm}(L_x, N)} Z_{0, i-\hat{x}} (Z_{2, i} Z_{2, i+\hat{y}}^{-1})^{i_x}, \\
\widetilde{W}_5 &= \prod_{i_y=1}^{L_y} Z_{1, i+\hat{x}} Z_{1, i}^{-1}, & \widetilde{W}_6 &= \prod_{i_x=1}^{L_x} Z_{2, i+\hat{y}} Z_{2, i}^{-1}.
\end{aligned} \tag{S19}$$

Upon initial inspection, the contributions of each logical operator on GSD appear as $\text{gcd}(L_y, N)$, N , N , $\text{gcd}(L_x, N)$, $\text{gcd}(L_x, N)$, and $\text{gcd}(L_y, N)$. The collective result of these contributions yields a GSD computation of $N^2[\text{gcd}(L_x, N) \text{gcd}(L_y, N)]^2$, which under-span the ground state Hilbert space.

The deficiency of the ground state basis comes from the fact that \widetilde{W}_4 given in above expression is not the most minimal choice of the logical operator. The correct logical operator expression is given by [19, 20]

$$\widetilde{W}_4^{\min} = \prod_{i_x=1}^{n_x L_x} Z_{0, i-\hat{x}} (Z_{2, i} Z_{2, i+\hat{y}}^{-1})^{i_x} \prod_{i_y=1}^{n_y L_y} Z_{0, i-\hat{y}} (Z_{1, i} Z_{1, i+\hat{x}}^{-1})^{i_y}, \tag{S20}$$

where the integers n_x and n_y are given by

$$n_x = \frac{\text{gcd}(L_y, N)}{\text{gcd}(L_x, L_y, N)}, \quad n_y = \frac{\text{lcm}(L_x, \text{gcd}(L_y, N)) + kN}{L_y}. \tag{S21}$$

Here, k is a minimal integer that makes n_y an integer [20]. The contribution of this logical operator corresponds to $N \text{gcd}(L_x, L_y, N) / \text{gcd}(L_y, N)$. Substituting \widetilde{W}_4 in Eq. (S19) with \widetilde{W}_4^{\min} yields the correct computation of GSD: $N^3 \text{gcd}(L_x, N) \text{gcd}(L_y, N) \text{gcd}(L_x, L_y, N)$.

The classification of six WW operators, which run along either the x -axis or the y -axis, can be easily done, except in situations where both L_x and L_y are not multiples of N . $\widetilde{W}_2, \widetilde{W}_4, \widetilde{W}_6$ are the product of Z 's along the x -axis and $\widetilde{W}_1, \widetilde{W}_3, \widetilde{W}_5$ are the product of Z 's along the y -axis. The results for the prime N are summarized in the Table I.

V. ENTANGLEMENT ENTROPY: CONTRACTIBLE BOUNDARY

The ground state we use for the calculation of entanglement entropy is $|\psi\rangle = |G|^{-1/2} \sum_{g \in G} g|0\rangle$, where G is generated by two magnetic stabilizers b_i^x and b_i^y . A naive estimate of $|G|$ for the group spanned by (b_i^x, b_i^y) on a $L_x \times L_y$ lattice is $N^{2L_x L_y}$, ignoring the constraint among the stabilizers. As noted in previous section, there are three

identities I_2, I_3, I_6 among the electric stabilizers that reduce the degree of freedom by factors of $N, N, \gcd(L_x, L_y, N)$, respectively, and therefore

$$|G| = N^{2L_x L_y} / (N^2 \gcd(L_x, L_y, N)). \quad (\text{S22})$$

We next compute $|G_A|$. We choose the region A to be a $l_x \times l_y$ square as shown in Fig. S2. The spins lying *on the boundary* are counted as living *inside* A . (Such ambiguities exist in defining the entanglement boundary of the ordinary toric code as well and are not new.) The number of b_i^x 's and b_i^y 's acting entirely within the region A is $N^{l_x(l_y-1)}$ and $N^{l_y(l_x-1)}$, respectively, and the cardinality of G_A follows

$$|G_A| = N^{l_x(l_y-1)} \times N^{l_y(l_x-1)} = N^{l_x(l_y-1)+l_y(l_x-1)}, \quad (\text{S23})$$

before considering the constraints among the stabilizers through the three identities $I_2 = I_3 = I_6 = 1$ defined throughout in Eqs. (S7) and (S8). Without loss of generality, however, we may pretend the non-independent stabilizers are living entirely in the region B and $|G_A|$ evaluated in (S23) is valid.

Now we come to the cardinality $|G_B|$. Ignoring the constraint among the stabilizers for the moment, counting the number of b_i^x, b_i^y stabilizers such that $b_i^x \notin G_B$ and $b_i^y \notin G_B$ (\notin means the stabilizer does not lie *entirely* within B , encompassing even those that are defined exclusively in set A .) gives $(l_x+1)(l_y+2)$ and $(l_x+2)(l_y+1)$, respectively, leading to the naive count $|G'_B| = |G|/N^{(l_x+1)(l_y+2)+(l_x+2)(l_y+1)}$. Note that in some cases an individual stabilizer does not lie fully inside B but their product does, and qualifies as an element of G_B . Explicitly, they are

$$\prod_{b_i^x \notin G_B} b_i^x \quad \prod_{b_i^y \notin G_B} b_i^y \quad \prod_{b_i^x, b_i^y \notin G_B} (b_i^x)^{-i_y} (b_i^y)^{i_x}. \quad (\text{S24})$$

Each product spans all the sites i for which the corresponding stabilizer does not lie fully inside the region B . One can readily check that the X operators in the interior cancel out, leaving only the product of X 's and X^\dagger 's along the one-dimensional loop closely following the boundary of A . Importantly, all the X operators that survive are located in the region B , and thus the three products in (S24) are indeed elements of G_B . The correct cardinality of G_B is greater than $|G'_B|$ evaluated above, and equals

$$|G_B| = |G'_B| \times N^3 = |G| N^{3-(l_x+1)(l_y+2)-(l_y+1)(l_x+2)}. \quad (\text{S25})$$

Combining the results of $|G|, |G_A|, |G_B|$ we arrive at the entanglement entropy of a disk-like bi-partition:

$$S_A = \log(|G|/(|G_A||G_B|)) = [4(l_x + l_y + 1) - 3] \log N. \quad (\text{S26})$$

The same calculation for the regular toric code gives $S_A = [2(l_x + l_y) - 1] \log N$, where $2(l_x + l_y)$ is interpreted as the length of the boundary and $\log N$ is the TEE. By comparison, the rank-2 calculation gives twice the geometric length, and an extra factor +1, with the TEE equal to $3 \log N$. We claim that a satisfactory interpretation of the factor $4(l_x + l_y + 1)$ is as the number of b_i^x and b_i^y 's that do not belong wholly to G_A or G_B , or *marginal stabilizers*. The extra factor 2 comes from having two types of stabilizers generating the group G . Such interpretation also nicely accounts for the extra +1 in the expression $4(l_x + l_y + 1)$, which is counting the correct number of marginal stabilizers. The factor 3 in the TEE is traced to the factor N^3 in the counting of $|G_B|$ as shown in (S25). In turn this comes from the three elements of G_B made out of stabilizers that do not belong wholly to G_B , as shown in (S24).

One can choose a different ground state $|\psi\rangle = |G|^{-1/2} \sum_{g \in G} g |+\rangle$, where $|+\rangle$ is a many-body product state satisfying $X_i |+\rangle = |+\rangle$ for all i . This time the group G is generated by stabilizers a_i . There are again three expressions, similar to (S24),

$$\prod_{a_i \notin G_B} a_i \quad \prod_{a_i \notin G_B} (a_i)^{i_x} \quad \prod_{a_i \notin G_B} (a_i)^{i_y}, \quad (\text{S27})$$

that become a product of Z 's and Z^\dagger 's in the B region along the boundary. Following the same procedure as before, we get

$$S_A = [4(l_x + l_y + 1) - 3] \log N, \quad (\text{S28})$$

identical to (S26) although there is only one type of generators a_i . Despite having only one stabilizer type, the same boundary term $4(l_x + l_y + 1)$ is obtained because a_i , compared to b_i^x, b_i^y is defined over a wider support [see (S5) for definition] and there are twice as many marginal a -stabilizers as there are marginal b^1 or b^2 stabilizers individually.

This also lends support to our previous interpretation of the leading factor $4(l_x + l_y + 1)$ as not just the geometric boundary, but as the number of marginal stabilizers.

It is easy to see that the TEE for the disk-like bi-partition will be the same for all other ground states generated by applying the WW operators W_1 through W_6 to the existing $|\psi\rangle$. All the WW operators $W_1 \sim W_6$ are defined along the non-contractible loops in the x - or y -direction. Without loss of generality we can make the assumption that all the WW operators act entirely within region B . When we again choose the same region A as in the previous entanglement entropy calculation using $|\psi\rangle$, the ratio $|G|/|G_B|$ for other ground states will remain consistent with that for $|\psi\rangle$. Furthermore, upon examining the elements of G_A , we observe that there is no element that can be represented as the product of $a_i \notin G_A$ and the WW operators. Consequently, the cardinality $|G_A|$ remains unchanged even with the inclusion of the WW operators as additional generators. As a result, the TEE will always be equal to $3 \log N$.

Furthermore, it is possible to show that the TEE result is same for the general ground states. The approach involves straightforwardly constructing the ground state $|\psi\rangle = |G|^{-1/2} \sum_{g \in G} g|0\rangle$, where G is generated by two magnetic stabilizers b_i^x and b_i^y . With this foundation in place, the general ground state can be represented as $\sum_i c_i O_i |\psi\rangle$, where O_i represents the element of the group generated by logical operators in X -operator basis and c_i stands for the coefficients. Using the fact that every logical operator can act exclusively within the region B , the reduced density matrix of region A , denoted as ρ_A^{gen} , can be similarly derived as in Sec. I:

$$\begin{aligned}
\rho_A^{\text{gen}} &= \text{Tr}_B \left[\sum_{i,j} c_i O_i |\psi\rangle \langle \psi| c_j^* O_j^\dagger \right] \\
&= |G|^{-1} \text{Tr}_B \left[\sum_{i,j} \sum_{g \in G, g' \in G} c_i O_i g |0\rangle \langle 0| (gg')^\dagger c_j^* O_j^\dagger \right] \\
&= |G|^{-1} \text{Tr}_B \left[\sum_{i,j} \sum_{g \in G, g' \in G} g_A |0\rangle_A \langle 0|_A (g_A g'_A)^\dagger \otimes c_i O_i g_B |0\rangle_B \langle 0|_B (g_B g'_B)^\dagger c_j^* O_j^\dagger \right] \\
&= |G|^{-1} \sum_{i,j} \sum_{g \in G, g' \in G} g_A |0\rangle_A \langle 0|_A (g_A g'_A)^\dagger \otimes \langle 0|_B (g_B g'_B)^\dagger c_j^* O_j^\dagger c_i O_i g_B |0\rangle_B, \tag{S29}
\end{aligned}$$

where $g = g_A \otimes g_B$ and $|0\rangle = |0\rangle_A \otimes |0\rangle_B$. The condition for $\langle 0|_B (g_B g'_B)^\dagger c_j^* O_j^\dagger c_i O_i g_B |0\rangle_B$ to become nonzero is $(g_B g'_B)^\dagger O_j^\dagger O_i g_B = 1$. Consequently, i must be the same as j , and $g'_B = I_B$. Ultimately, the expression for ρ_A can be simplified to:

$$\rho_A^{\text{gen}} = |G|^{-1} \sum_{g \in G, g' \in G_A} g_A |0\rangle_A \langle 0|_A (g_A g'_A)^\dagger, \tag{S30}$$

where $G_A = \{g \in G | g = g_A \otimes I_B\}$, and ρ_A^{gen} is equal to ρ_A in (S3). Therefore, the EE and the TEE of the general ground state remain identical to those of the state $|\psi\rangle$.

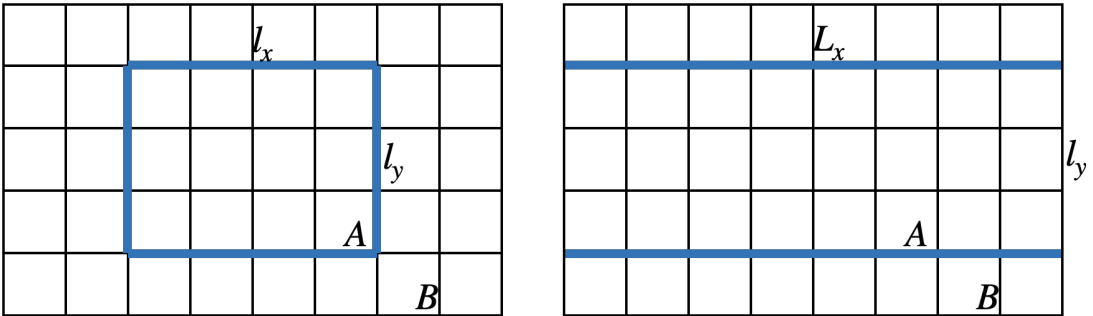


FIG. S2: Figure of region A with (left) contractible boundary and (right) x -cut.

VI. ENTANGLEMENT ENTROPY : NON-CONTRACTIBLE BOUNDARY

Consider now the region A defined by two non-contractible boundaries running along the x -axis and of width l_y , with the area given by $L_x \times l_y$. The MES for the x -cut (non-contractible boundaries running along the x -axis of the

torus) is constructed as $|\psi_{\text{MES}}\rangle = |G_{\text{MES}}|^{-1/2} \sum_{g \in G_{\text{MES}}} g|0\rangle$, where the group G_{MES} is spanned by b_i^x, b_i^y , and three WW operators W_1, W_3, W_5 . The state thus constructed is an eigenstate of W_1, W_3, W_5 and the logical operators which are running along the x -axis and in Z -operator basis. Therefore, the state qualifies as MES [28].

Given that the degeneracy factors of W_1, W_3 , and W_5 are $N \gcd(L_x, L_y, N) / \gcd(L_x, N)$, N , and $\gcd(L_x, N)$, respectively, the cardinality of G can be expressed as $N^{2L_x L_y}$. The reason the degeneracy factor of the WW operator is not N is that only the WW operators with specific exponents are considered logical operators. Without loss of generality, we assume that the dependent stabilizers are situated in region B . Furthermore, there are two regions near the boundaries where neither b_i^x nor b_i^y belongs to both G_A and G_B . We assume that the WW operators are positioned in one of these regions located above region A , and we denote this region as region AB . This arrangement ensures that there are no dependent stabilizers between the WW operators and the boundary of region A .

In this case, the TEE is determined by determined by two types of operations: (i) the operation in G_B , which can be expressed as the product of $b_i^x, b_i^y \notin G_B$ (ii) the operations in G_A , which can be expressed as the product of $b_i^x, b_i^y \notin G_A$, and the WW operators W_1, W_3, W_5 located in region AB . First of all, the operations that satisfy the former conditions are

$$\prod_{b_i^x \notin G_B} b_i^x \quad \prod_{b_i^y \notin G_B} b_i^y \quad \left(\prod_{b_i^x, b_i^y \notin G_B} (b_i^x)^{-i_y} (b_i^y)^{i_x} \right)^{c_x}. \quad (\text{S31})$$

The first two expressions are identical to those of (S24). The third expression is that of (S24) raised to $c_x = N/\gcd(L_x, N)$ to take account of the periodic boundary conditions for b_i^y . To be faithful to the periodic boundary condition one must be able to impose $(X_0)^{L_x} \equiv 1$ but this is not always the case. On the other hand, $(X_0)^{c_x L_x} \equiv 1$ is always true and the number of additional elements in G_B is $N^2 \gcd(L_x, N)$ instead of N^3 . Therefore, the cardinality of $|G_B^x| = |G| N^2 \gcd(L_x, N) / N^{L_x(l_y+2)+L_x(l_y+1)}$.

We have identified four operations that fulfill the latter conditions, with three of them being expressed as:

$$W_1 \prod_{b_i^x \in G_{AB}} b_i^x \quad W_3 \prod_{b_i^y \in G_{AB}} b_i^y \quad W_5 \prod_{b_i^x \in G_{AB}} (b_i^x)^{-i_y}. \quad (\text{S32})$$

Here, G_{AB} consists of elements of G that have support exclusively within region AB . The stabilizers cancel out the X 's of WW operators acting on the region B , leaving the remaining operators located on region A . The degeneracy factor of three operations in (S32) is same with the degeneracy factors of W_1, W_3 , and W_5 . The last operation which satisfy the latter condition is well defined when W_1 with particular exponent k is not a logical operator. This implies that W_1^k can be represented as the product of b_i^x and b_i^y . In that case, we can still find W_1^k located in the region AB within the group G . However, $W_1^k \prod_{b_i^x \in G_{AB}} b_i^x$ does not satisfy the latter conditions since W_1^k includes the product of $b_i^x, b_i^y \in G_A$. Here, we need to focus on the fact that when we express W_1^A as the product of $b_i^x, b_i^y \in G_A$ included by W_1 , the following expression:

$$W_1^k (W_1^A)^\dagger \prod_{b_i^x \in G_{AB}} b_i^x \quad (\text{S33})$$

definitely satisfies the latter condition. We cannot find another operation when W_3 or W_5 is not a logical operator. This is because W_3 is always a logical operator regardless of the lattice size, and when W_5 is not a logical operator, it is effectively the same as W_3 . Therefore, the degeneracy factors related to W_1, W_3 , and W_5 are N, N , and $\gcd(L_x, N)$, respectively, and the cardinality of G_A^x is $N^{L_x(2L_y-1)} N^2 \gcd(L_x, N)$. The results can be summarized:

$$\begin{aligned} |G| &= N^{2L_x L_y} \\ |G_A^x| &= N^{L_x(2L_y-1)} N^2 \gcd(L_x, N) \\ |G_B^x| &= |G| N^2 \gcd(L_x, N) / N^{L_x(l_y+2)+L_x(l_y+1)} \\ S_A^x &= 4L_x \log N - \log(N^4 \gcd(L_x, N)^2). \end{aligned} \quad (\text{S34})$$

Through a similar calculation, the entanglement entropy S_A^y for the non-contractible boundary along the y -direction is given by $S_A^y = 4L_y \log N - \log(N^4 \gcd(L_y, N)^2)$.

We consider the MES characterized by eigenvalues of $+1$ for all logical operators aligned with the x (y)-axis in the case of the x (y)-cut, from which we derive the TEE result. It can be shown that the MES with different eigenvalues for corresponding logical operators have the same TEE. This is because the general MES can be described by $U |\psi_{\text{MES}}\rangle$, where U is the product of logical operators along the y (x)-axis in the case of x (y)-cut. Given that $U = U_A \otimes U_B$

and $|\psi_{\text{MES}}\rangle = |G|^{-1/2} \sum_{g \in G} g_A |0\rangle_A \otimes g_B |0\rangle_B$, the reduced density matrix of region A for a general MES, denoted as ρ_A , is expressed as follows:

$$\begin{aligned}
\rho_A &= \text{Tr}_B[U |\psi_{\text{MES}}\rangle \langle \psi_{\text{MES}}| U^\dagger] \\
&= \text{Tr}_B\left[\sum_{g, g' \in G} U_A g_A |0\rangle_A \langle 0|_A (g_A g'_A)^\dagger U_A^\dagger \otimes U_B g_B |0\rangle_B \langle 0|_B (g_B g'_B)^\dagger U_B^\dagger\right] \\
&= \sum_{g \in G, g' \in G_A} U_A g_A |0\rangle_A \langle 0|_A (g_A g'_A)^\dagger U_A^\dagger \\
&= U_A \rho_A^{\text{MES}} U_A^\dagger,
\end{aligned} \tag{S35}$$

where ρ_A^{MES} is the reduced density matrix of region A for the original MES state. Hence, $\text{Tr}_A[\rho_A^n] = \text{Tr}_A[(\rho_A^{\text{MES}})^n]$, which implies that the EE outcomes for general MES are consistent with (8) for the x -cut and (9) for the y -cut.

VII. TEE AND GSD CALCULATION USING SYMMETRY DEFECT THEORY

In the framework of symmetry defect theory, we explicitly calculate the TEE of R2TC using (16). To count the number of \mathbf{h} - or \mathbf{g} -invariant anyons among the a_0 anyons in (1), we should consider how they transform when they move around the torus:

$$\begin{aligned}
l_{L_x+i_x, i_y} &= l_{i_x, i_y} + (l_1 L_x \bmod N) \mathbf{p}^x - (l_5 L_x \bmod N) \mathbf{g} \\
l_{i_x, L_y+i_y} &= l_{i_x, i_y} + (l_1 L_y \bmod N) \mathbf{p}^y + (l_4 L_y \bmod N) \mathbf{g}.
\end{aligned} \tag{S36}$$

Clearly, anyons in $C_0^{\mathbf{h}}$ must satisfy $l_1 L_x \bmod N = 0 = l_5 L_x \bmod N$, that is, l_1 and l_5 must be multiples of $N/\text{gcd}(L_x, N)$. Since the other four integers are \mathbb{Z}_N without restriction, we find $|C_0^{\mathbf{h}}| = N^4 \text{gcd}(L_x, N)^2$, in agreement with γ_{MES}^x in (8). A similar reasoning correctly captures γ_{MES}^y .

We calculate the GSD of R2TC using (18) in two steps: first identify distinct defects in $C_{\mathbf{g}}$, then further identify those that are invariant under the symmetry defect \mathbf{h} . Since any one of the defect in $C_{\mathbf{g}}$ can be obtained from any other by fusing it with some anyon, and we can find at least one defect $a_{\mathbf{g}} \in C_{\mathbf{g}}$ which is \mathbf{h} -invariant, we can express general defects in $C_{\mathbf{g}}$ as $a_{\mathbf{g}} \otimes l_{i_x, i_y}$. Not all of these defects are necessarily distinct; we need to find a minimal set of anyons that, when fused with $a_{\mathbf{g}}$, generates all distinct defects in $C_{\mathbf{g}}$. To this end, we employ the known property that all defects in $C_{\mathbf{g}}$ are automatically \mathbf{g} -invariant [10]. The statement of \mathbf{g} -invariance becomes

$$a_{\mathbf{g}} \otimes l_{i_x, i_y} = \mathbf{g}(a_{\mathbf{g}} \otimes l_{i_x, i_y}) = a_{\mathbf{g}} \otimes \mathbf{g}(l_{i_x, i_y}) = a_{\mathbf{g}} \otimes l_{i_x, L_y+i_y}. \tag{S37}$$

Using (S36), we can equivalently state (S37) as

$$a_{\mathbf{g}} \otimes (l_1 L_y \bmod N) \mathbf{p}^y \otimes (l_4 L_y \bmod N) \mathbf{g} = a_{\mathbf{g}}. \tag{S38}$$

The coefficients before \mathbf{p}^y and \mathbf{g} mean the number of such anyons that, when fused with $a_{\mathbf{g}}$, becomes the $a_{\mathbf{g}}$ itself. For instance, $L_y \bmod N$, $2L_y \bmod N$, etc. number of \mathbf{p}^y or \mathbf{g} anyons have such a property. By Bezout's identity, this number is lower-bounded by $\text{gcd}(L_y, N)$ for both \mathbf{p}^y and \mathbf{g} . Then, by limiting the number of \mathbf{p}^y, \mathbf{g} anyons to be less than $\text{gcd}(L_y, N)$, we obtain the desired expression of quasiparticles in $C_{\mathbf{g}}$, denoted as $l_{i_x, i_y}^{\mathbf{g}}$:

$$\begin{aligned}
l_{i_x, i_y}^{\mathbf{g}} &= l_1 \mathbf{e} + ((l_1 i_x + l_2) \bmod N) \mathbf{p}^x + ((l_1 i_y + l_3) \bmod \text{gcd}(L_y, N)) \mathbf{p}^y \\
&\quad + l_4 \mathbf{m}^x + l_5 \mathbf{m}^y + ((l_4 i_y + l_5 i_x + l_6) \bmod \text{gcd}(L_y, N)) \mathbf{g},
\end{aligned} \tag{S39}$$

where the coefficients before \mathbf{p}^y and \mathbf{g} are both mod $\text{gcd}(L_y, N)$ rather than mod N , as was in (1). The number of distinct $l^{\mathbf{g}}$ -anyons is equal to $|C_{\mathbf{g}}|$ and is $N^4 \text{gcd}(L_y, N)^2$.

The subset of $C_{\mathbf{g}}$ that are \mathbf{h} -invariant satisfies $l_{i_x, i_y}^{\mathbf{g}} = l_{L_x+i_x, i_y}^{\mathbf{g}}$ since $a_{\mathbf{g}}$ was assumed to be \mathbf{h} -invariant. Then, we can get

$$l_1 L_x \bmod N = 0 = l_5 L_x \bmod \text{gcd}(L_y, N). \tag{S40}$$

This implies that l_1 and l_5 must be multiples of $N/\text{gcd}(L_x, N)$ and $\text{gcd}(L_y, N)/\text{gcd}(L_x, L_y, N)$, respectively. Counting the distinct set of integers $l_1 - l_6$ in (S39) consistent with (S40), we find $|C_{\mathbf{g}}^{\mathbf{h}}| = \text{GSD}$. Similar consideration applies to $|C_{\mathbf{h}}^{\mathbf{g}}|$ with the same result.

VIII. SPURIOUS ENTANGLEMENT ENTROPY

We analyze the spurious entanglement of the non-topological model proposed in [41], using our idea of taking the bulk product of stabilizers to arrive at the boundary product. We conclude the boundary product in this case does not fully encircle the region A , and also find some dependence on the shape of the boundary.

The model [41] is defined on a square lattice, comprising two stabilizers:

$$a = \begin{array}{c} IZ - IZ \\ | \quad | \\ IZ - XZ \end{array} \quad b = \begin{array}{c} ZX - ZI \\ | \quad | \\ ZI - ZI. \end{array} \quad (\text{S41})$$

Two \mathbb{Z}_2 degrees of freedom are assigned to each vertex corresponding to the first and the second Pauli operator in the above. The (unique) ground state of this model is

$$|\psi\rangle = |G|^{-1/2} \sum_{g \in G} g |0+\rangle, \quad (\text{S42})$$

where the group G is generated by a 's and $|0+\rangle$ satisfies $IX|0+\rangle = ZI|0+\rangle = |0+\rangle$ for arbitrary vertices.

We evaluate the entanglement entropy of $|\psi\rangle$ first for a $l_x \times l_y$ square region A as depicted in Fig. S2. The operations that significantly influence the TEE are the elements of G_B , which are the product of $a \notin G_B$, and the elements of G_A , which are the product of $a \notin G_A$. We can identify the operation satisfying the former condition, depicted in Fig. S3 (a). The operation is the multiplication of a 's and encircled by the yellow loop. This operation in terms of X and Z takes the form of a square bracket encompassing a part of the boundary, signifying that the count of such operations is expected to vary based on the shape of the region. The entanglement entropy result is summarized as

$$\begin{aligned} |G| &= 2^{L_x L_y} \\ |G_A| &= 2^{l_x l_y} \\ |G_B| &= |G| 2^{-(l_x+2)(l_y+2)+1} \\ S_A &= (2l_x + 2l_y) \log 2 - \log 2, \end{aligned} \quad (\text{S43})$$

and TEE is equal to $\log 2$. We can easily check that the TEE depends on the shape of the boundary. By altering the boundary, as depicted in Fig. S3 (b), we can identify two operations influential to the TEE, each one encircled by yellow loop.

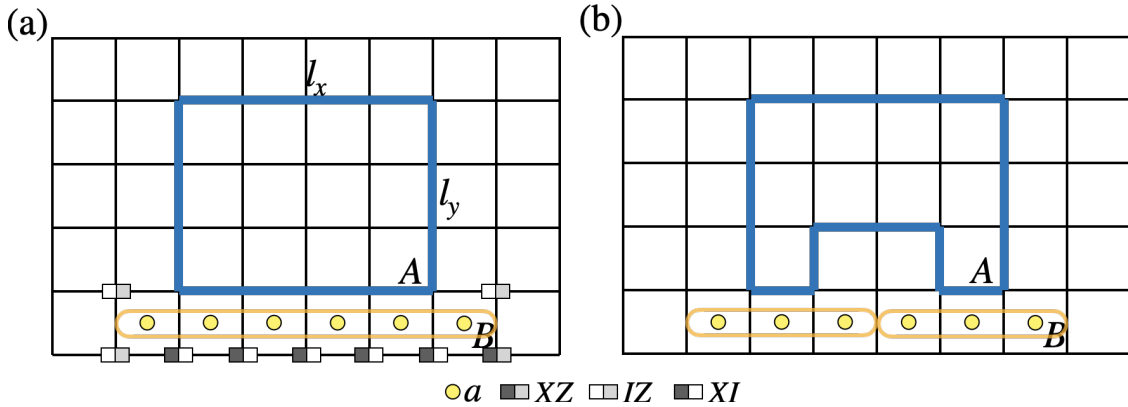


FIG. S3: (a) An operation satisfying the condition of being an element of G_B and the product of $a \notin G_A$. The operation is influential to the TEE and represented by the encircled yellow loop. (b) Two operations, represented by yellow loops and influential to the TEE, are depicted.

This observation deviates from the well-known concept of TEE and should be regarded as spurious TEE. Conversely, if the operation takes the form of a WW loop encircling the entire boundary of the region, the number of elements cannot depend on the shape of the region, indicating a genuine TEE. Based on the analysis conducted in this simple example, we can confidently assert that there are no instances of spurious TEE in the entanglement entropy calculation for R2TC. The identified operations are the the form of WW loop, thereby eliminating any possibility of spurious TEE contributions.

IX. TENSOR NETWORK CALCULATION: ENTANGLEMENT ENTROPY FOR R2TC

In this section, we demonstrate how to express the MES of R2TC using a Tensor Network (TN) framework, building upon the TN wavefunction introduced in Ref. 19. By examining the local gauge symmetry of tensors as summarized in Ref. 19, when both system sizes L_x and L_y are multiples of N , the TN wavefunction serves as a ground state of R2TC and is simultaneously an eigenstate of $W_1, W_2, W_3, W_4, \widetilde{W}_5$, and \widetilde{W}_6 , all with eigenvalues equal to 1. However, when we consider a y -cut, the MES should be an eigenstate for the WW operators $\widetilde{W}_1, W_2, \widetilde{W}_3, W_4, \widetilde{W}_5$, and W_6 simultaneously. Therefore, the TN wavefunction originally proposed in Ref. 19 is not an MES and requires some modifications to transform it into an MES.

The process of modifying the TN wave function to become a MES for y -cut can be broken down into three distinct steps. The first step is to enforce TN wavefunction to be an eigenstate of \widetilde{W}_1 instead of W_1 . In the second step, we make further modifications to the TN to ensure wavefunction to be an eigenstate of \widetilde{W}_3 instead of W_3 . Finally, in the third step, we enforce the wavefunction to be eigenstate of W_6 instead of \widetilde{W}_6 .

A. Review: Tensor network wavefunction

In this subsection, we review the TN wavefunction introduced in Ref. 19, which is suggested as one of the TN formulas responsible for one of the R2TC ground states. The TN wavefunction is composed of three local tensors $T_{udlr}, g_{udlr}^{s_1 s_2}$, and $g_{udlr}^{s_0}$ and can be represented as below:

$$(S44)$$

The indices s_1, s_2, s_0 represent physical indices corresponding to the local \mathbb{Z}_N orbitals of R2TC, while the indices u, d, l, r are virtual indices with \mathbb{Z}_N character that are contracted out in the final expression. The first two tensors are defined as

$$T_{udlr} = \delta_{u+r-(l+d), 0}, \quad g_{udlr}^{s_1 s_2} = (\delta_{l,r} \delta_{l,s_1}) (\delta_{d,u} \delta_{d,s_2}). \quad (S45)$$

Note that the delta is implemented by mod N throughout this section. To define the third local tensor, we need to introduce following isometry tensor:

$$P_{s_1 s_1}^{s_0} = \delta_{s_0, s_1 + s_2}. \quad (S46)$$

Then the third local tensor is defined as

$$g_{udlr}^{s_0} = P_{s_1 s_1}^{s_0} g_{udlr}^{s_1 s_2}. \quad (S47)$$

Here, the summation for repeated indices is implied.

B. Loop-gas interpretation

As mentioned in above, the TN wavefunction is an eigenstate of WW operators without tilde; W_1, W_2, W_3 , and W_4 . To gain an intuitive understanding of this, we introduce the concept of a loop-gas configuration picture. From this point onward, we confine our analysis to the \mathbb{Z}_2 case for the sake of clarity and simplicity in the subsequent discussion. The concepts and principles discussed can be readily extended to the general \mathbb{Z}_N case without any

difficulty. Furthermore, our discussion will primarily center on scenarios where both system sizes, L_x and L_y , are even. To say it in advance, we have numerically confirmed that the TN achieved by the discussion below also serves as a MES for system size under various conditions.

In \mathbb{Z}_2 case, one can understand the virtual legs as being occupied by a loop when the corresponding virtual index has a value of 1, and being unoccupied when the value is 0. Using this interpretation, we can translate the TN wavefunction in Eq. (S44) into the loop-gas configuration picture. In doing so, we discover that the TN wavefunction is essentially an equal superposition of every possible closed-loop configurations, both on the solid and dotted lattices, respectively. An example of the closed-loop configuration is given in Fig. S4 (a).

This is attributed to the role played by T_{udlr} , which acts to ensure the closure of all loops. It is because, from the definition of T_{udlr} in Eq. (S45), whenever a loop enters to T_{udlr} , it must also exit. It is important to note that the closed-loop condition enforced by T_{udlr} facilitates the presence of non-contractible loop configurations around the torus system.

Now, we consider how the WW operator W_1 acts on the TN wavefunction. To see that, we need to understand the action of a local Pauli- X operator on the g tensors. Referring to the definition in Eq. (S45), one can observe that when $s_1 = 1$ ($s_2 = 1$), a solid (dotted) line crossing the $g_{udlr}^{s_1 s_2}$ tensor is occupied by a horizontal (vertical) loop, while it remains empty when $s_1 = 0$ ($s_2 = 0$). Additionally, for either the dotted or solid lines crossing the $g_{udlr}^{s_0}$, they are occupied by horizontal or vertical lines when $s_0 = 1$, and both lines are either empty or occupied by both horizontal and vertical lines when $s_0 = 0$. Consequently, applying a local Pauli- X operator to the g tensors leads to a switch in the occupation state as described.

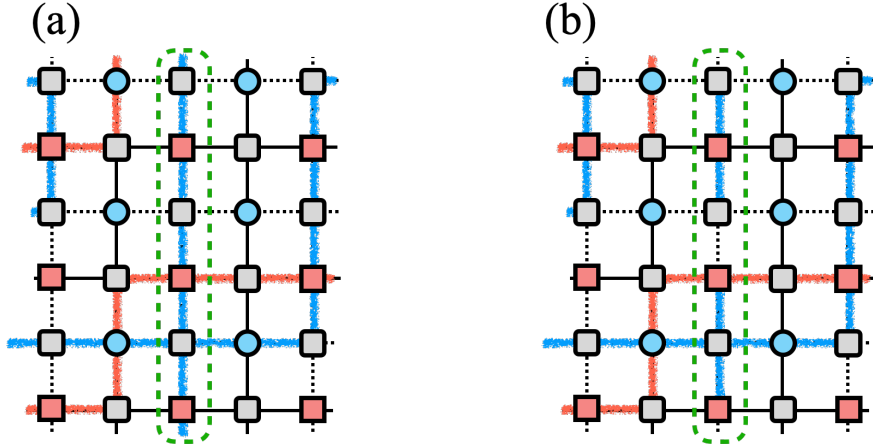


FIG. S4: Illustrations of R2TC loop configurations. Blue lines denote loops on the dotted lattice, while orange lines represent loops on the solid lattice. The physical indices are omitted. The position where W_6 is applied is marked by closed green dashed-loop. (a) A configuration comprising exclusively of closed loops. (b) A configuration featuring a single isolated vertical loop. All other loops, apart from the vertical one at rightmost dotted column, are closed.

The WW operator W_1 acts by applying Pauli- X operators to lattice sites positioned on the non-contractible dotted line defined along the x -axis. Building upon the insights from the previous paragraph, it becomes clear that the action of W_1 involves the insertion of a horizontal non-contractible loop in the dotted lattice. It is worth noting that in the context of our \mathbb{Z}_2 system, the insertion of a non-contractible loop is equivalent to toggling the number of non-contractible loops between even and odd. Since the TN wave function described in Eq. (S44) already includes all possible closed loop configurations, encompassing both cases containing an even or odd number of non-contractible loops, the operations performed by the W_1 operator do not alter the TN wave function. This property results in the TN wavefunction being an eigenstate of W_1 with an eigenvalue of 1. By applying a similar rationale as discussed above, one can ascertain that the remaining WW operators, W_2 , W_3 , and W_4 also function by inserting horizontal or vertical non-contractible loops into the dotted or solid lattices, respectively. Employing analogous logic, it can be deduced that the TN wavefunction defined in Eq. (S44) is likewise an eigenstate of W_2 , W_3 , and W_4 with an eigenvalue of 1.

Now we will delve into the three steps involved in transforming the TN wavefunction into an MES within the framework of loop-gas configurations, addressing each step individually. The first step is to enforce it to be an eigenstate of \widetilde{W}_1 instead of W_1 . These operators are in anti-commutation relation: $W_1 \widetilde{W}_1 = -\widetilde{W}_1 W_1$. We shall now represent the eigenstates of \widetilde{W}_1 with the eigenvalues 1 and -1 , as $|0\rangle$ and $|1\rangle$, respectively. We use the representations 0 and 1 to emphasize that the tilde WW operator \widetilde{W}_1 is composed of the product of Pauli- Z operators. The action of W_1

interchanges these two states, transforming $|0\rangle$ into $|1\rangle$ and vice versa. The eigenstates of W_1 can be expressed as an equal superposition of these two states, taking the form of $1/\sqrt{2}(|0\rangle \pm |1\rangle)$ with eigenvalue ± 1 . The TN wavefunction is an eigenstate of W_1 with eigenvalue 1, and hence taking form $1/\sqrt{2}(|0\rangle + |1\rangle)$. Furthermore, combining with the discussion of the closed-loop configuration above, it can be inferred that either $|0\rangle$ or $|1\rangle$ correspond to an equal superposition of every closed loop configuration, with the distinction being that they contain either an even or odd number of horizontal non-contractible loops in the dotted lattice.

Enforcing the TN wavefunction to be an eigenstate of \widetilde{W}_1 can be understood as transforming the original wavefunction from the form $(|0\rangle + |1\rangle)$ into either $|1\rangle$ or $|0\rangle$. In the loop-gas configuration picture, this translates to ensuring that the TN wavefunction contains either an even or odd number of horizontal non-contractible loops in the dotted lattice. This marks the first step in the process of making the TN wavefunction an MES.

Expanding on this idea, one can observe that enforcing the TN wavefunction to be an eigenstate of \widetilde{W}_3 is equivalent to guaranteeing that the TN wavefunction comprises only even or odd numbers of horizontal non-contractible loops in the solid lattice. This step is evidently the second stage in the modifying the TN wavefunction into an MES.

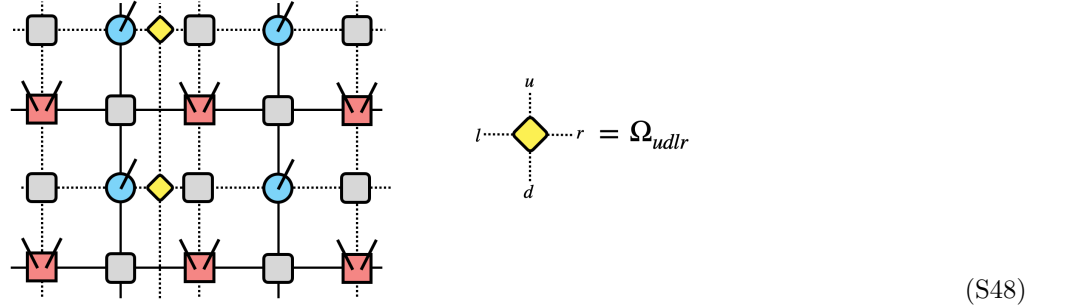
The final step involves ensuring that the TN becomes an eigenstate of W_6 instead of being an eigenstate of \widetilde{W}_6 . The original TN wave function given in Eq. (S44) consists solely of closed-loop configurations as in Fig. S4(a). However, when we apply W_6 , it introduces a vertical dashed line on the dotted lattice, as illustrated in Fig. S4(b).

Let's consider the anti-commutation relation $W_6\widetilde{W}_6 = -\widetilde{W}_6W_6$. The eigenstates of \widetilde{W}_6 are denoted as $|0\rangle$ and $|1\rangle$, corresponding to eigenvalues 1 and -1 , respectively. The action of W_6 interchanges these two states, transforming $|0\rangle$ into $|1\rangle$ and vice versa. Consequently, it can be deduced that the original TN wavefunction takes the form of $|0\rangle$, whereas the TN wavefunction containing a single vertical dashed line on the dotted lattice, denoted as $W_6|0\rangle$, takes the form of $|1\rangle$.

Since the MES is required to be an eigenstate of W_6 , we must ensure that it takes the form of $|0\rangle \pm |1\rangle$. This is equivalent to constructing the TN as a superposition of two sets of loop configurations. One set consists solely of closed-loop configurations (Fig. S4(a)), while the other includes a single vertical dashed loop on the dotted lattice (Fig. S4(b)). This completes the final step of transforming the original TN wavefunction into an MES.

C. Tensor network implementation

In the following, we will provide a detailed explanation of how to implement these three steps within the framework of TN one by one. In first step, we need to ensure that the TN wavefunction only contains even-number of horizontal non-contractible closed loop on dotted lattice. This can be simply done by pick any single vertical line form dotted lattice. Then attaching a new tensor Ω_{udlr} to T_{udlr} tensors located on the vertical line as



Here, the tensor Ω_{udlr} is defined by

$$\Omega_{udlr} = \delta_{l,r} \delta_{l,u-d}. \quad (\text{S49})$$

To grasp how the tensor Ω_{udlr} constrains the quantity of horizontal non-contractible closed loops, let's focus on a vertical dotted bond connected to Ω_{udlr} . Let's assume we initiate with a value of 0 for the virtual bond and traverse along the y -direction. Whenever we encounter a horizontal loop that crosses through Ω_{udlr} , the value of the vertical bond toggles between 0 and 1, and vice versa. If a configuration contains an odd number of non-contractible horizontal loops on the dotted lattice, we will encounter the horizontal loop an odd number of times during the round trip, causing the virtual bond to end up with a value of 1. Since the initial value of the virtual bond was 0, this scenario leads to a mismatch and is therefore excluded from the tensor contraction. Consequently, we obtain configurations that exclusively consist of an even number of horizontal non-contractible loops on the dotted lattice.

Similarly, by additionally attaching Ω_{udlr} to T_{udlr} tensors located at any single vertical line form solid lattice as

$$(S50)$$

Note that in the remaining vertical lattice lines, Ω_{udlr} is not connected. As a result, the TN wave function now exclusively comprises loop configurations with an even number of horizontal non-contractible loops on each lattice. This condition ensures that the TN wave function becomes an eigenstate of both \widetilde{W}_1 and \widetilde{W}_3 marking the successful completion of the first and second steps.

The implementation of third step, the final step of enforcing the TN wavefunction being an MES, encompass not only just attaching additional auxiliary tensor, involves more than just the attachment of an additional auxiliary tensor. It also necessitates the modification of certain local tensors T_{udlr} . Similar to the first and second step, we pick a single vertical lines from dotted lattice, and replace the tensors T_{udlr} with $T_{udlr;m}$, which can be graphically illustrated as

$$T_{udlr;m} = \begin{array}{c} u \\ \vdots \\ \square \\ \vdots \\ d \end{array} \begin{array}{c} l \cdots \cdots r \\ \vdots \\ m \end{array} = \begin{array}{c} u \\ \vdots \\ \text{slanted square} \\ \vdots \\ d \end{array} \begin{array}{c} l \cdots \cdots r \\ \vdots \\ m \end{array} . \quad (S51)$$

Here, the first image provides a top view, while the second offers a side view from a slanted perspective. The leg representing \mathbb{Z}_2 index m goes the direction penetrating the surface, in contrary to the physical indices in Eq. (S44) comes in the direction emerging from the surface. Its mathematical definition is given by

$$T_{udlr;m} = \delta_{u+r-(l+d),m}, \quad (S52)$$

Now, $T_{udlr;m}$ allows termination of a loop at the point when $m = 1$. Note that $T_{udlr;0} = T_{udlr}$.

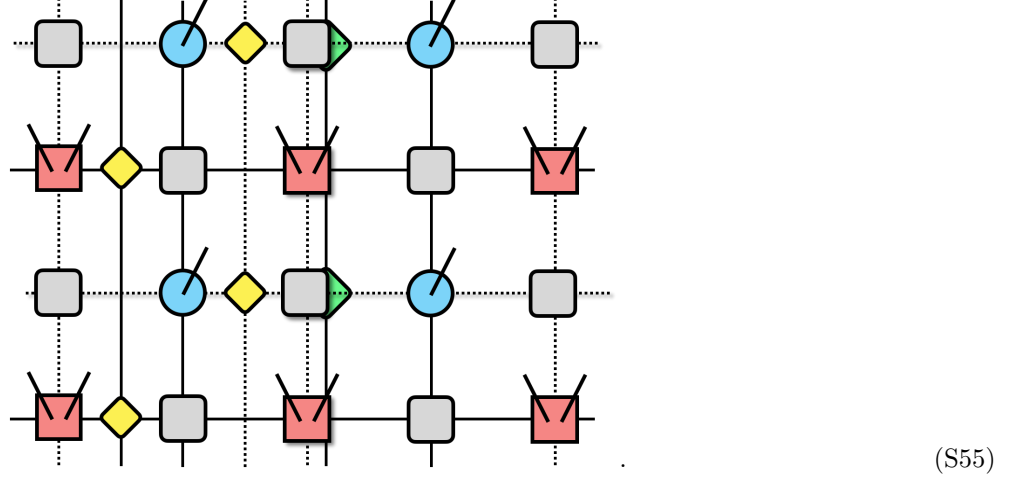
Afterward, we attach the $\Theta_{u'd'}^m$ right below the $T_{udlr;m}$ as

$$\sum_m T_{udlr;m} \Theta_{u'd'}^m = \begin{array}{c} u \quad u' \\ \vdots \\ \square \\ \vdots \\ d \quad d' \end{array} \begin{array}{c} l \cdots \cdots r \\ \vdots \\ m \end{array} = \begin{array}{c} u \\ \vdots \\ \text{slanted square} \\ \vdots \\ d \end{array} \begin{array}{c} l \cdots \cdots r \\ \vdots \\ m \end{array} \begin{array}{c} u' \\ \vdots \\ \text{green diamond} \\ \vdots \\ d' \end{array} . \quad (S53)$$

Here, $\Theta_{u'd'}^m$ is defined by

$$\Theta_{u'd'}^m = \delta_{m,u'} \delta_{u,d'} \quad (S54)$$

Consequently, the ultimate structure of the TN wave function takes the form:



With the introduction of $\Theta_{u'd'}^m$, we introduce an additional vertical line on the “lower level” of the original lattice, linking the indices u' and d' . As defined in Eq. (S54), this vertical line allows only two configurations: either a closed non-contractible loop occupies the line, or the line remains empty. The configurations of the empty line correspond to the configurations prior to the third step. In the case of an occupied line, the configurations encompass a single vertical dashed loop on the dotted lattice, as depicted in Fig. S4(b). This completes the entire step of transforming the TN wavefunction into a MES.

Numerically, we have confirmed that the wavefunction constructed by the TN given in Eq. (S55) is MES for any cases of system size. Specifically, we have calculated the expectation values for WW operator in Table I being 1 for the TN wavefunction.